

Predictive and feedback signals differently shape the formation of group-level and individualized language representations

Shuguang Yang ^{1,2}, Shaoyun Yu ^{3,4}, Xin Jiang ^{1,2}, Suiping Wang ^{1,2}, Gangyi Feng ^{3,4*}

1. School of Psychology, South China Normal University, Guangzhou 510631, China
2. Philosophy and Social Science Laboratory of Reading and Development in Children and Adolescents (South China Normal University), Ministry of Education, Guangzhou 510631, China
3. Department of Linguistics and Modern Languages, The Chinese University of Hong Kong, Hong Kong SAR, China
4. Brain and Mind Institute, The Chinese University of Hong Kong, Hong Kong SAR, China

* Corresponding author

Gangyi Feng

Brain and Mind Institute

Department of Linguistics and Modern Languages

The Chinese University of Hong Kong, Hong Kong SAR, China.

Email: g.feng@cuhk.edu.hk

Funding

The work described in this paper was supported by grants from the National Natural Science Foundation of China (Project No. 32322090 to Gangyi Feng), the Research Grants Council of the Hong Kong Special Administrative Region, China (Project No.: 14614221, 14612923, 14621424, and C4001-23YF to Gangyi Feng), and Key Research and Development Program of Guangdong, China (grant number: 2023B0303010004 to Suiping Wang).

Conflict of interest statement

The authors declare no competing financial interests.

Abstract

Adults vary greatly in how effectively they learn a new language, but the signals driving the learning processes and individual differences remain unclear. Over seven days, we tracked behavioral learning and collected fMRI data from 102 adults as they learned an artificial language with corrective feedback. We trained matched transformer models with prediction, feedback, or combined objectives and compared their internal representations to brain activity. Representations derived from the prediction-focused model accounted for the largest share of unique neural variance at the group level, despite the human task being feedback-based. Throughout model training, both objectives showed a shift in brain-model alignment from sensory to higher-order language and associative networks, indicating abstraction processing. Conversely, neural patterns related to the feedback model were most useful for predicting individual generalization outcomes on Day 7. These findings support a multi-signal model of adult language learning, in which prediction shapes a common neural learning architecture across learners, whereas feedback-related mechanisms better explain individual differences over time.

Keywords: language learning, individual differences, prediction, feedback signals, neural systems

Introduction

Adults often spend years learning a new language, yet progress is often slow, effortful, and varies greatly among individuals. Even with similar instruction and exposure, some learners rapidly extract linguistic regularities and generalize them to new contexts, whereas others improve more slowly or reach only modest levels of proficiency (Kidd et al., 2018; Krishnan et al., 2016; Morgan-Short, 2020). Understanding the language learning process and its variability is key to understanding human learning, as it affects not only language acquisition but also how the adult brain builds new, structured knowledge from experience.

A longstanding debate centers on whether adult language learning is driven primarily by a single learning process or by multiple signals that contribute differently depending on the learning demand (Minda et al., 2024; Morgan-Short, 2020; Hamrick et al., 2018; Ullman, 2004; Ashby et al., 1998). Two candidates are especially prominent. One highlights prediction-based learning, where learners track distributional structure in the input and form expectations about upcoming sounds, words, and syntactic structures. This enables them to build representations that support generalization across different contexts and time frames (Caucheteux et al., 2023; Heilbron et al., 2022; Pelucchi et al., 2009; Saffran, 2002; Saffran et al., 1996). The other underscores feedback-based learning, in which explicit correctness signals and outcome-dependent adjustments help learners refine responses and acquire abstract constraints. This account emphasizes the role of cortico-striatal systems involved in sequential and category learning (Feng, Gan, et al., 2021; Feng, Ou, et al., 2021; Krishnan et al., 2016; Schultz et al., 1997), processes that may support the acquisition of grammatical constraints. Both perspectives are plausible, but it remains unclear how these learning signals shape the formation of language representations and whether they matter differently for the common neural organization versus individual differences among learners.

This uncertainty persists in part because the two accounts are usually studied separately. Prediction-based learning is often examined using statistical learning or self-supervised language modeling (Bovolenta & Marsden, 2022; Ito et al., 2018; Rabagliati et al., 2015), whereas feedback-based learning is typically studied using supervised or reinforcement-like paradigms (Arbel et al., 2014, 2017). These different approaches use different tasks, models, and outcome measures, making direct comparison challenging. As a result, three questions remain unresolved. First, does adult language learning rely on multiple learning signals instead of a single dominant mechanism? Second, do these signals contribute differently across brain systems and across stages of learning? Third, can these differences explain why some learners generalize successfully while others do not?

We addressed these questions using a unified framework to compare candidate learning signals in a common computational and representational space. Transformer models are particularly useful for this purpose. Classical symbolic, feature-engineered and statistical models have provided important mechanistic insights, but they typically

rely on hand-crafted representations or modular pipelines that are less suited to capturing end-to-end representational change during learning (Elman, 1990; Naselaris et al., 2011; Riesenhuber & Poggio, 1999). By contrast, transformer models can be trained with different objectives on the same corpus, yielding directly comparable internal representations within a shared architecture. Recent work has also shown that such representations align with human neural activity across the cortical hierarchy during language processing (Caucheteux et al., 2022, 2023; Goldstein et al., 2022). This makes them a powerful tool for testing where, when, and to what extent distinct learning objectives resemble the representational geometry of the human brain.

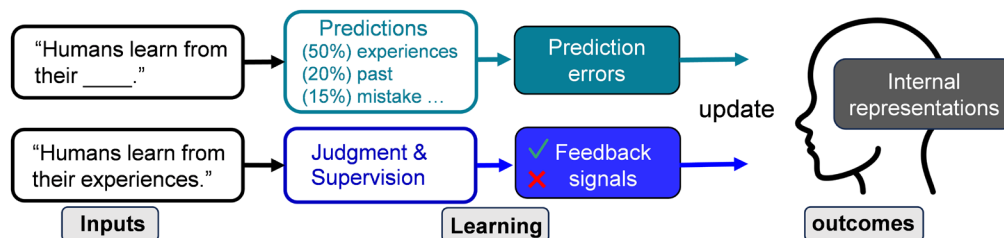
A key conceptual point is that the current models focus on learning signals rather than fully implementing entire theoretical frameworks. Specifically, we operationalize the prediction objective as next-token prediction and the feedback objective as correctness-supervised grammaticality judgment using a trial-wise feedback structure. These objectives capture distinct learning pressures. The prediction objective imposes an *internally* generated pressure to anticipate upcoming structure from distributional regularities, whereas feedback imposes an *externally* provided pressure to update responses based on success and error signals. Therefore, they should not be viewed as direct, one-to-one implementations of predictive coding theory (Friston, 2005) or algorithmic reinforcement learning (Sutton & Barto, 2018) in their strongest forms. Instead, they serve as controlled approaches to test whether representations optimized for prediction and feedback objectives relate differently to human neural activity and behavior. This distinction is especially important because prediction can either be a driver of language learning or an emergent byproduct of it (Chang et al., 2006, 2013). Thus, this comparative framework allows us to manipulate learning objectives while keeping the model architecture and training materials constant, enabling us to measure how the resulting internal representations correspond to neural activity during human learning. It also allows us to test whether mechanism-related neural information can better predict individual learning outcomes.

We applied this framework to a seven-day artificial-language learning study using Brocanto2, a miniature artificial language with a controlled lexicon and grammar embedded in a meaningful board-game context (Morgan-Short et al., 2010, 2012). We tracked behavioral learning in 102 participants over the full training period and collected fMRI data on Day 1, while participants learned Brocanto2 with corrective feedback. In parallel, we trained three GPT-style models with the same architecture but different objectives (Fig. 1). One was a prediction model (GPT-P) optimized for next-token prediction, another was a feedback model (GPT-F) optimized for grammaticality judgment with corrective feedback, and the third was a combined model (GPT-PF) optimized for both tasks. We then aligned trained model representations with fMRI data using representational similarity analysis (RSA) and variance partitioning, tracked stage-specific representational updates across training, and built individualized multimodal models that combined early neural and behavioral information to predict generalization performance on Day 7.

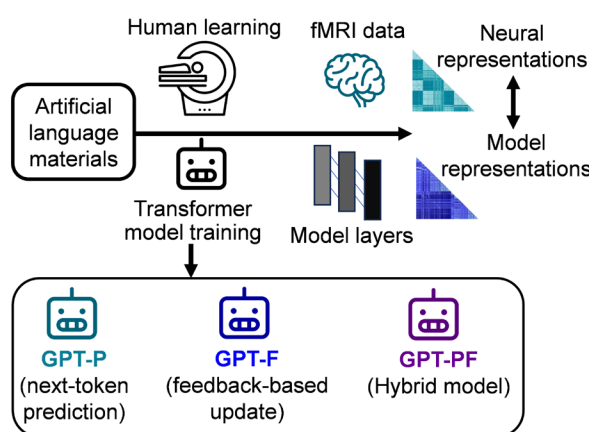
This design enabled us to test three specific predictions. First, if prediction-based learning provides a dominant representational scaffold, representations optimized for a prediction objective should explain more unique neural variance at the group level than those optimized for the feedback objective, despite the human task being feedback-based. Second, if model representations become more abstract during training, as they do in humans, then model-brain alignment should shift from lower-level sensory systems to higher-order language and associative networks. Meanwhile, these shifting patterns may vary between the two model types. Third, if learner-specific outcomes depend more on how learning signals are encoded and used, then neural information related to a given learning signal should better predict later individual differences in generalization to unseen items.

By combining prediction- and feedback-based objectives within a common computational and neuroimaging framework, this study reframes the debate over adult language learning from a competition between single mechanisms to a question of functional dissociation. We demonstrated that prediction-based representations best explain the neural geometry shared across learners, whereas feedback-related neural information best predicts individual differences in later generalization. These findings suggest that adult language learning is not governed by a single dominant signal, but by partially complementary learning signals that operate at different levels of explanation. More broadly, our approach establishes model-brain alignment as a mechanistic assay for testing how adults acquire new structured knowledge and why learners exposed to the same language input arrive at different outcomes.

a Multiple-learning signals



b Model-brain alignment procedure



c Individualized learner modeling

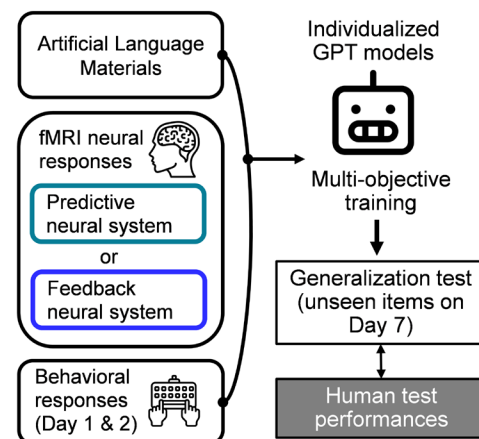


Fig. 1. Overview of the study framework and procedure. a, Hypothesized learning

mechanisms supporting human language learning. The framework compares two candidate signals: prediction, based on next-element prediction among alternatives, and feedback-based learning, based on outcome signals (correct or incorrect). Both update the internal representations of language. **b**, Model-brain alignment procedure. Participants learned an artificial language while fMRI data were collected, and parallel GPT models were trained on the language materials. Three models were compared: GPT-P (next-token prediction), GPT-F (feedback-based learning), and GPT-PF (both). RSA compared model layers' representations with neural responses. **c**, Individualized learner modeling. To explain individual differences in learning, participant-specific GPT models combined artificial-language materials with early behavioral responses and neural responses from prediction or feedback neural systems. These models predicted Day-7 generalization performance on unseen items. This approach examines which learning mechanism and neural system best explain the variation in language-learning success.

Results

Human and model language-learning performance

We collected fMRI data on Day 1 from 102 adults performing an artificial language-learning task that required grammaticality judgments with trial-by-trial corrective feedback. Participants then completed six additional days of behavioral training using the same paradigm, followed by a Day 7 generalization test that assessed grammaticality knowledge on unseen items (Fig. 2a).

To test the candidate learning mechanisms, we trained three small-scale GPT-style models with identical architectures and hyperparameters, differing only in their training objectives. Each model used a two-layer decoder-only architecture, comprising one token-embedding layer and two hidden layers. GPT-P was trained for next-token prediction using cross-entropy loss. GPT-F was trained on the grammaticality-judgment task with explicit correctness feedback. GPT-PF combined both objectives by jointly optimizing prediction and feedback objectives with dynamic loss weighting (see Methods). This design allowed us to isolate the contribution of each mechanism and test whether combining them improved model performance and alignment with human data.

All three models reached a performance plateau within 200 training epochs. GPT-P achieved 91% validation accuracy in generating unseen grammatical sentences, and GPT-F reached 100% accuracy on grammaticality judgments. GPT-PF surpassed the single-objective GPT-P model in sentence generation (96%) while closely matching GPT-F in grammaticality judgment (97%) (Fig. 2c). In addition, grammaticality judgment in both GPT-F and GPT-PF exceeded human learners' Day-7 peak accuracy (79%; Fig. 2b and Supplementary Fig. S1).

To examine how the models' capabilities emerged, we tested whether changes in their internal layer representations predict changes in their task performance across

training checkpoints (see Methods and Fig. S2). We computed representation-update RDMs and performance-update RDMs, as well as their associations, for all three models (Fig. 2d). In GPT-P, we found significant associations across all layers, though weaker than in GPT-F. In GPT-F, the associations were robustly positive and strongest in the two hidden layers, indicating tighter coupling between representation updating and performance improvement. In GPT-PF, representational updates were positively related to both sentence generation and grammaticality judgment performance, with the effects increasing over layers. Thus, learning in all three models involved systematic reorganization of internal representations relevant to the tasks.

We next compared representational geometry across models (Fig. 2e). Among model pairs, GPT-P and GPT-F showed the lowest similarity between corresponding hidden layers ($r_{\text{layer1}} = 0.081$, $r_{\text{layer2}} = 0.076$), indicating that prediction- and feedback-based objectives produced distinct internal representations. Although GPT-PF shared the same architecture as the two single-objective models, its layer representations were more similar to GPT-F ($r_{\text{layer1}} = 0.357$, $r_{\text{layer2}} = 0.543$) than to GPT-P ($r_{\text{layer1}} = 0.298$, $r_{\text{layer2}} = 0.272$), especially in Layer 2. This pattern suggests that the combined model retains a stronger feedback-related representational signature while still incorporating prediction-based structure.

We then examined how GPT-P and GPT-F aligned with human learning behavior (i.e., responses) across model training (Fig. 2f). For this analysis, we constructed a mean behavioral-response RDM from human judgment patterns across the seven training days and compared it with model RDMs extracted from four checkpoints sampled at comparable intervals of performance improvement along each model’s training trajectory. These checkpoints divided each model’s training trajectory into comparable stages of improvement. In Layer 1, GPT-P showed stronger model-behavior alignment at the early stages (i.e., the first two checkpoints: $p = 2.82 \times 10^{-3}$ and 4.56×10^{-5}), did not differ reliably from GPT-F at the third checkpoint ($p = 0.34$), and was weaker than GPT-F at the final checkpoint ($p = 1.99 \times 10^{-21}$). In Layer 2, GPT-P remained more strongly aligned through the first three checkpoints ($p = 2.60 \times 10^{-6}$, 1.80×10^{-6} , and 6.60×10^{-3}), whereas GPT-F showed stronger alignment at the final checkpoint ($p = 3.11 \times 10^{-15}$). These results reveal a temporal shift in model-human-behavior alignment, in which early-to-intermediate prediction-based representations better captured human learning behaviors, whereas later feedback-based representations better captured behavior as model performance approached the asymptote.

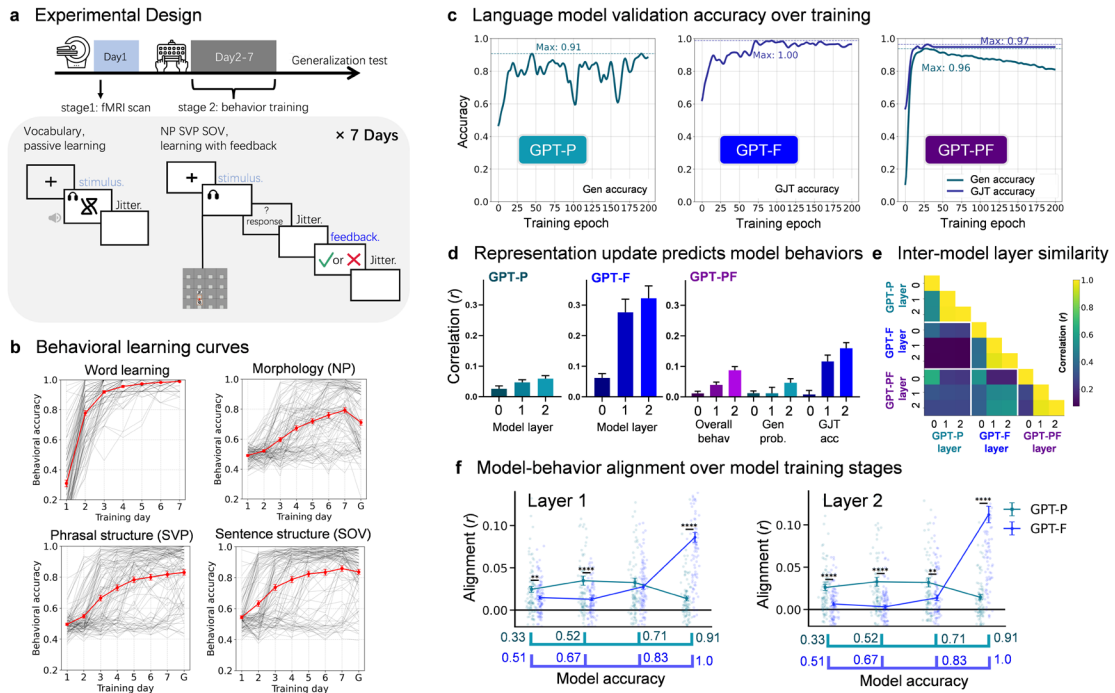


Fig. 2. Experimental design, behavioral learning curves, and model-behavior alignment. **a**, Seven-day training and neuroimaging procedure. Participants underwent fMRI on Day 1 during vocabulary and grammar training, followed by behavioral training on Days 2-7, ending with a generalization test. **b**, Behavioral learning curves over the 7 training days for word, morphology, phrasal, and sentence structure. Gray lines represent individual participants; red lines show the group means. G = generalization scores. **c**, Validation performance of the three models across training epochs. For GPT-P and GPT-PF, performance is displayed as the rate of generating novel grammatical sentences (“Gen accuracy”); for GPT-F and GPT-PF, grammaticality judgment test (GJT) accuracy is shown. **d**, Associations between model representational and behavioral change are shown with bar plots of Spearman correlations between representational-update RDMs and performance-update RDMs across layers and models. **e**, Similarity of internal representations across models. The heat map displays layer-wise correlations between model RDMs. **f**, Model-to-human-behavior representation alignment. Mean RSA alignment (r) between model representations and human behavioral patterns is shown across four model checkpoints. Dots indicate individual participants, and error bars indicate SEM. Asterisks indicate paired t -test results for the comparison between GPT-P and GPT-F at each stage. **, $p < 0.01$; ****, $p < 0.0001$.

Predictive representations accounted for most neural variance during learning

We next examined how closely the representational geometry of the three models aligned with human neural RDMs during learning. To this end, we used whole-brain searchlight RSA (Kriegeskorte, 2008; Stolier & Freeman, 2016) with multiple regression (Fig. 3a) to reveal the unique contribution of each model. Layer-wise RDMs from the models were fitted to predict fMRI-derived RDMs while controlling for three

nuisance RDMs (i.e., an untrained GPT model, stimulus length, and block identity). We further complemented whole-brain RSA with variance partitioning (Groen et al., 2018) and network-wise RSA across 12 canonical functional brain networks (Ji et al., 2019).

All three models showed reliable alignment with human neural representations (Fig. 3b and see Fig. S3 for layer-wise RSA maps). However, the extent and distribution of this alignment differed across models. Although the human task focused on grammaticality judgments with feedback, the GPT-P model accounted for the greatest amount of neural variance (Fig. 3c). As a control, we trained an additional GPT-P(L) model with a training set size matched to that of the human task (288 items) and still observed consistent and robust model-brain alignment (Fig. S4). This alignment also extended beyond cortical regions to subcortical structures, including the caudate, nucleus accumbens and globus pallidus, consistent with evidence for a contribution of the basal ganglia to language learning (Krishnan et al., 2016). By contrast, the feedback model (GPT-F) aligned with human data closely in canonical perisylvian language regions (Hagoort, 2019) and the default mode network (Menon, 2023), whereas the integrated model (GPT-PF) showed additional alignment only in early sensorimotor cortices.

These between-model differences were further supported by variance partitioning. GPT-P accounted for the largest share of unique neural variance across model layers (Fig. 3c). We then examined whether the models differed in their alignment with neural representations extracted from 12 canonical brain networks. Consistent with the overall variance-partitioning results, GPT-P showed significantly higher alignment than the other models in most networks (8 of 12; paired *t*-tests; Fig. 3d). GPT-F did not significantly outperform GPT-P in any network. These converging results indicate that prediction-based representations provide the strongest group-level account of neural patterns during human language learning.

To investigate how feedback-based grammaticality training shapes representational geometry relative to classic reinforcement-like reward learning, we trained two control models: GPT-R, a policy-gradient reinforcement-learning counterpart to GPT-F, and GPT-PR, a combined prediction-plus-policy-gradient counterpart to GPT-PF. This was crucial because GPT-R may achieve comparable task performance by maximizing reward, yet produce very different internal representations than GPT-F. We conducted the same multiple regression analysis, replacing GPT-F and GPT-PF's layer-wise RDMs with those of GPT-R and GPT-PR, while holding the other regressors constant. Although GPT-R achieved similar model accuracy to GPT-F, its internal representations did not significantly align with human neural activity ($p > 0.05$; Fig. 3b, dashed box, see also Supplementary Fig. S5 for more details). These results suggest that reward-based training alone was insufficient to approximate the neural representational geometry observed during human language learning.

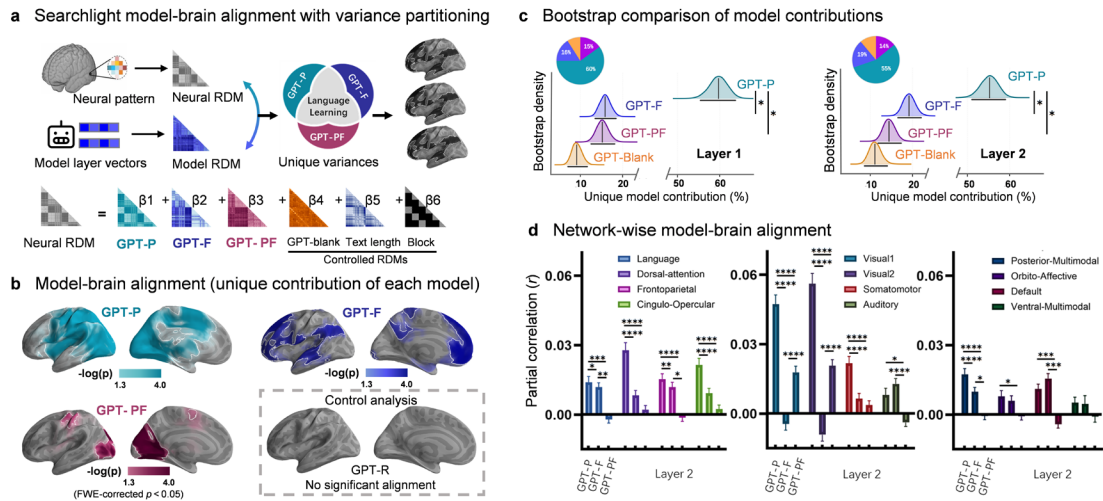


Fig. 3. Whole-brain and network-wise RSA dissociate the contributions of prediction and feedback-based learning. **a**, Schematic overview of the whole-brain searchlight RSA and variance-partitioning procedure. At each searchlight location, neural RDMS were regressed against model RDMS to estimate the contributions of the models to neural representations, controlling for an untrained GPT baseline (GPT-Blank), text length, and experimental block. **b**, Whole-brain searchlight RSA results for models' layer 2. In the control analysis (dashed box), the policy-gradient reinforcement model (i.e., GPT-R) showed no significant alignment, despite robust model performance (see Fig. S5). Brain maps were thresholded using TFCE with 10,000 permutations and family-wise-error corrected $p < 0.05$. **c**, Bootstrap comparison of relative RDM contributions. Bootstrap distributions of the proportion of total explained variance attributable to each model RDM across the first and second model layers. Each bootstrap sample's R^2 for each model RDM is shown as a percentage of the total R^2 from GPT-P, GPT-F, GPT-PF, and GPT-Blank. Density plots show resampled contribution estimates, with horizontal lines for central tendency and asterisks indicating significant differences. **d**, Network-wise RSA across 12 canonical functional networks for the models' layer 2. Bars show partial correlations between neural and model RDMS for each network, controlling for the other RDMS. Prediction-based representations showed the strongest alignment across sensorimotor, language, and association networks, whereas feedback-based representations contributed more selectively. *, $p < 0.05$; **, $p < 0.01$; ***, $p < 0.001$; ****, $p < 0.0001$.

Overall, these findings support the multiple learning signal account of language learning and are difficult to reconcile with strong accounts in which prediction is unnecessary (Huettig & Mani, 2016) or merely epiphenomenal during language learning (Chang et al., 2013). Instead, prediction-based representations provide a dominant account of the group-level neural geometry observed during early adult language learning, even when the human learning task is feedback-oriented.

Human-like abstract model representations emerge progressively across training along a bottom-up cortical gradient

To determine when and how model representations become more human-like over the course of model training, we performed RSA on representation updates rather than on static representations alone. Because human fMRI data were available only from Day 1, the neural RDMs served as a fixed reference for the brain’s representational geometry during early acquisition, rather than a temporally matched series across learning. We therefore used successive model checkpoints to identify when, in model training, the model’s internal changes began to resemble this early human learning state.

We sampled four checkpoints at similar intervals of improvement in validation accuracy, thereby dividing training into three stages (Fig. 4a and see Methods for details). For each stage, we computed representational change vectors and derived RDMs summarizing the geometry of these updates. We focused on the update RDMs rather than the checkpoint RDMs to examine the emergence of human-like representations during model training, not simply their presence at particular stages. Checkpoint RDMs capture the cumulative representational state of the model and therefore may conflate newly acquired structure with the geometry inherited from earlier training. In contrast, update RDMs can avoid this conflation by characterizing how representations change between training stages. This approach made it possible to examine when and how models acquire human-like representational geometry.

We found that human-like model representations emerged progressively rather than simultaneously across brain regions. The emerging pattern followed a bottom-up cortical gradient, moving from lower-level sensory systems toward higher-order language and associative systems (Fig. 4b). For GPT-P, alignment gradually shifted from primary cortical regions to the language and default mode networks across training (Fig. 4b, lower panel), indicating that the model first captured relatively low-level or surface representational structure and only later acquired representational structures resembling those in higher-order systems.

To quantify representational alignment trajectories, we assessed changes in alignment across 12 brain networks. In GPT-P (Fig. 4c), alignment decreased across training stages in lower-order regions such as the secondary visual network, while increasing in higher-order systems such as the language and associative networks (Fig. 4d-e). GPT-F showed a qualitatively similar but weaker and delayed pattern. Alignment first appeared in lower-order systems at the middle stage, with significant effects in the secondary visual network and the adjacent ventral multimodal network. Subsequently, this alignment extended toward higher-order cortical systems at the late stage.

To further quantify these model differences in temporal dynamics, we fitted a linear regression model to each participant’s partial alignment values across the three training stages, separately for each model and network. These estimated per-subject slopes index the rate at which model-brain alignment changed over training. In both the language and default mode networks, GPT-P exhibited significantly steeper positive slopes than GPT-F (Fig. 4e), indicating that GPT-P not only achieved stronger overall alignment but also acquired update patterns more rapidly, resembling those of higher-order human brain systems.

In summary, these findings reveal when and how model representations become human-like. Models' alignment with human brain data emerged gradually, following a bottom-up trajectory from sensory toward higher-order networks. Both prediction- and feedback-based learning showed evidence of this progression, but with different temporal profiles. GPT-P showed robust alignment with brain activity across all stages, indicating that prediction supports the emergence of human-like representations. GPT-F showed weaker and slower-emerging alignment, suggesting that feedback-based learning may require more extensive training to acquire comparable representational similarity.

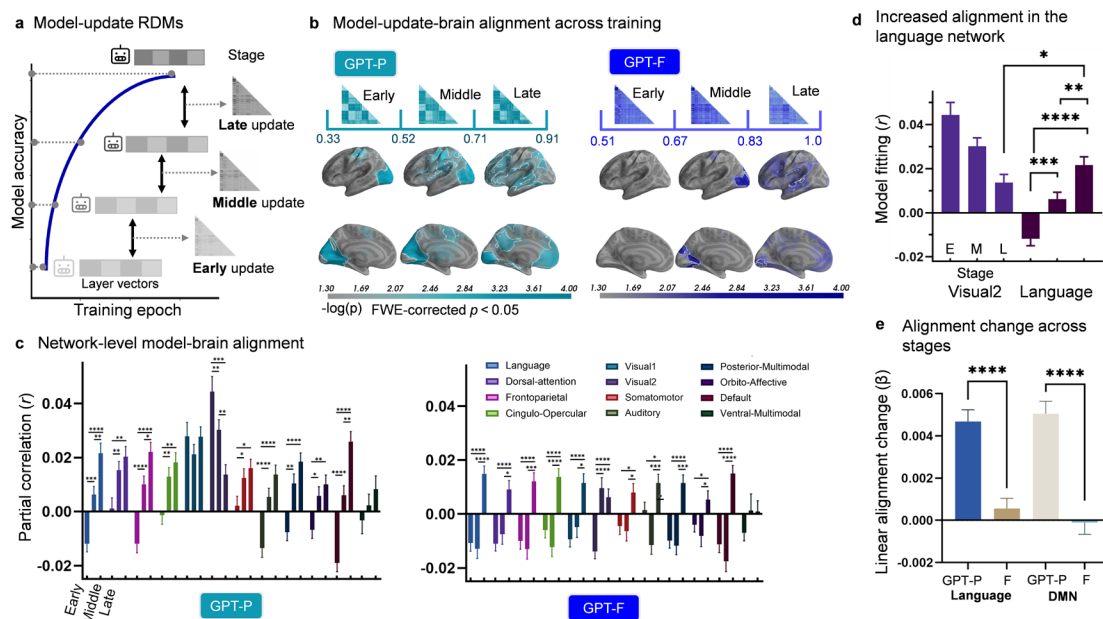


Fig. 4. Model-brain representational alignment shifts from sensorimotor to language and higher-order systems. **a**, Schematic showing representation-update-based brain-model alignment analysis. Vector representations were sampled at multiple points during model training, and changes were measured as the differences between adjacent checkpoints to construct the update RDM. This captures how internal model geometry updates across training stages. **b**, Whole-brain RSA results for representational updates in the first layer of GPT-P and GPT-F across three successive training stages. The numbers below the brain maps show model performance for sampled checkpoints. Brain maps are thresholded using TFCE with 10,000 permutations and FWE-corrected $p < 0.05$. **c**, Network-wise RSA of representational updates across training stages for both models. Bars show partial correlations between neural RDMs and stage-specific update RDMs across the 12 functional networks. **d**, Direct comparison of GPT-P update alignment in the secondary visual (Visual2) and language networks. **e**, Linear slopes fitted to each participant's stage-wise update alignment values. GPT-P showed significantly larger increases than GPT-F in both the language and default mode networks, indicating a stronger late-emerging shift towards

higher-order representational systems. *, $p < 0.05$; **, $p < 0.01$; ***, $p < 0.001$; ****, $p < 0.0001$.

Individualized neurocomputational models identify the predictors of individual differences

We further examined which learning-related signals better explain individual differences in final learning outcomes. To address this question, we developed individualized GPT models trained on each participant's early behavioral and neural responses (Fig. 5a). Each model was trained with three sources of information: next-token predictions, individual learners' grammaticality judgment responses, and individual neural features extracted from selected brain regions. By comparing models constrained by different neural features (from GPT-F- or GPT-P-related brain regions), we tested whether feedback- or prediction-related neural signals better predicted learners' later generalization to unseen materials.

These individualized models successfully captured both neural and behavioral responses (Fig. 5b-c). When trained with neural objectives, they showed greater similarity to participant-specific neural responses than the behavioral-only model (Fig. 5c). We next tested whether these early learning signals could predict individual generalization to unseen materials on Day 7. While early behavioral data provided limited predictive power ($r = 0.27$), incorporating neural constraints improved prediction significantly, reaching a cross-validated predictive power of $r = 0.43$ ($p < 0.001$; Fig. 5d). In bootstrap comparisons, the model trained with feedback-related neural regions (derived from the GPT-F's RSA map with the update RDMs) significantly outperformed the behavioral-only model ($p < 0.001$), whereas the model trained with prediction-related neural regions did not ($p = 0.17$; Fig. 5e). The feedback-region model also outperformed the prediction-region model ($p = 0.047$), indicating that feedback-related neural information was more informative than prediction-related neural signals for explaining individual differences in later generalization.

This advantage was not attributable to differences in voxel count between the brain masks. The feedback mask initially contained fewer voxels than the prediction mask. To rule out a simple volumetric explanation, we conducted a control analysis in which the statistical threshold for the feedback-region mask was adjusted to yield a voxel count closely matched to that of the prediction-region mask (Supplementary Fig. S6a). Using this voxel-matched mask, we repeated the full individualized modeling procedure. The feedback-region model continued to significantly predict Day 7 generalization performance (Spearman $r = 0.41$, $p = 2.37 \times 10^{-5}$; Supplementary Fig. S6d), and in bootstrap comparisons, it remained significantly superior to the behavioral-only baseline ($p = 0.0031$; Supplementary Fig. S6e).

Together, these findings show that individualized neurocomputational models can help identify the mechanisms underlying individual differences in language learning success. By training participant-specific neural-enhanced language models under different neural constraints and testing their ability to predict subsequent generalization,

we found that feedback-related neural signals were more informative than prediction-related signals in explaining why learners differed in their generalization outcomes. These results extend the group-level analyses by suggesting that prediction and feedback make complementary contributions to language learning.

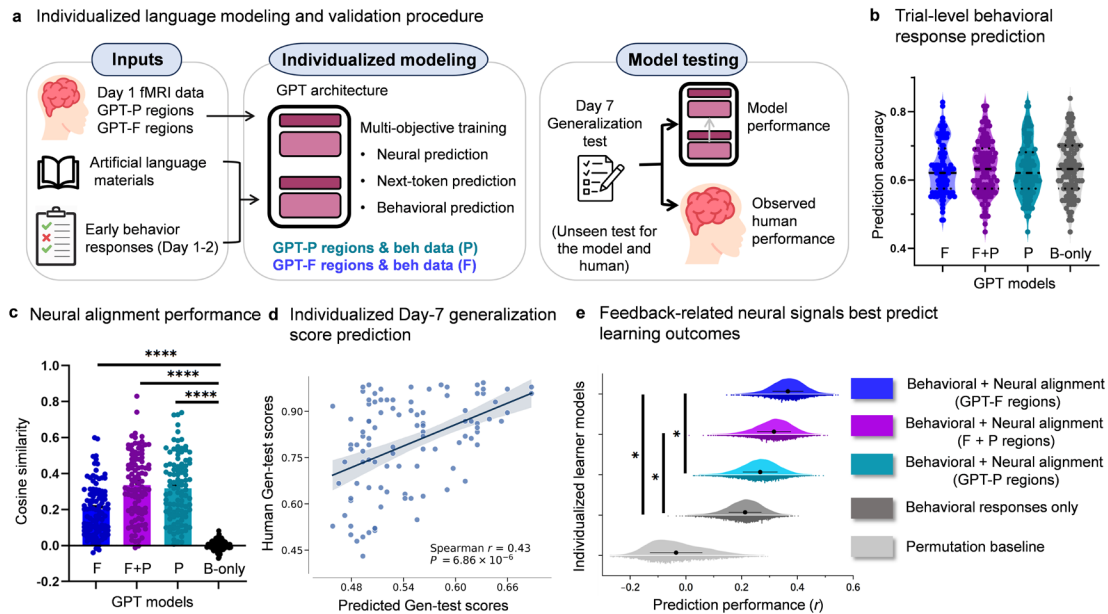


Fig. 5. Individualized models predict later generalization from early behavioral and neural data. **a**, Schematic of the individualized modeling framework. Participant-specific models were trained on next-token prediction (using Brocanto2 materials), early behavioral responses, and Day 1 fMRI-derived neural features from prediction-related regions, feedback-related regions or both. **b**, Trial-level behavioral response prediction across individualized models. **c**, Cosine similarity between model representations and participant-specific neural representations. Models trained with neural objectives showed greater neural alignment than the behavioral-only model. **d**, Prediction of Day 7 generalization scores by the best-performing individualized model. **e**, Bootstrap distributions of prediction performance for the generalization test. Models using feedback-related neural regions or the combined neural mask outperformed the behavioral-only model, whereas the model using prediction-related neural regions did not. The feedback-region model also outperformed the prediction-region model. *, $p < 0.05$; ****, $p < 0.0001$.

Discussion

Using a seven-day artificial-language-learning paradigm, fMRI recordings during early learning, and the development of group-level and individualized transformer models, we found that prediction and feedback explain complementary aspects of adult language learning. Prediction-based representations best captured neural structure shared across learners, whereas feedback-related neural signals better explained individual differences in later generalization. At the group level, representations optimized for a prediction objective accounted for the largest portion of unique explainable neural variance, even though participants performed a feedback-based learning task. Throughout training, both prediction-based and feedback-based representations showed a bottom-up shift from sensory regions toward higher-order language and associative networks, with a stronger shift for the prediction model than for the feedback model. At the individual level, early feedback-related neural responses improved the prediction of Day 7 generalization task performance beyond that of the prediction model and the behavior-only model. Overall, these findings support a multi-signal account of adult language learning, in which prediction primarily shapes the neural representational structure shared across learners, whereas feedback-related signals better explain why learners later diverge in learning performance.

The group-level findings are most informative when interpreted in light of the learning objectives implemented. Next-token prediction operationalized a prediction-based learning signal, whereas a grammaticality judgment task with trial-by-trial corrective feedback operationalized a feedback-based learning signal. These objectives should not be viewed as complete implementations of predictive-coding theory or reinforcement learning in an algorithmic sense. However, within this operationalization, our results are consistent with prediction-related computations providing a representational scaffold during even early learning. Prediction has been connected to both language learning and processing, with evidence that learners use distributional regularities to anticipate upcoming linguistic structures and that hierarchical predictive signals can be detected across the cortical language system (Caucheteux et al., 2023; Heilbron et al., 2022; Pelucchi et al., 2009; Saffran, 2002; Saffran et al., 1996). At the same time, prediction has also been argued to arise as a byproduct rather than a driver of learning (Chang et al., 2006, 2013). Our results do not fully settle this broader debate, but they do provide an important constraint. Even in a task designed around explicit correctness feedback, representations optimized for prediction showed the strongest model-brain alignment and explained the largest proportion of unique explainable variance. This pattern is more consistent with the view that prediction-related signals are actively involved in updating representations during learning than with the view that they are merely epiphenomenal.

This interpretation is also consistent with recent work showing that predictive structure is a major source of alignment between deep language models and human brain activity during language processing (Caucheteux et al., 2022, 2023; Goldstein et al., 2022). In that sense, our findings extend the relevance of prediction beyond mature

language comprehension to the formation of new linguistic knowledge. Importantly, the current findings do not imply that prediction alone suffices for effective language learning. Instead, they indicate that prediction-related processes significantly influence the neural representational structure across learners.

The complementary role of feedback-related signals is equally important. Adult language learning is often supported by explicit correctness information, and outcome-based updating has long been linked to cortico-striatal systems involved in sequential learning, category learning, and aspects of grammar acquisition (Feng, Gan, et al., 2021; Feng, Ou, et al., 2021; Krishnan et al., 2016; Schultz et al., 1997). In our data, however, feedback-related representations did not dominate the neural geometry across learners. Instead, they were most informative in explaining individual differences in later learning success. Individualized neural-constrained language models that integrate feedback-aligned neural targets outperformed models focused on early behavioral-response and prediction-aligned brain regions in predicting Day-7 generalization. This result indicates that feedback could be particularly valuable for understanding how learners leverage information about errors and correctness to refine their internal models or decision-making strategies over time.

The stage-specific representational update findings suggest that prediction- and feedback-based signals are embedded in a common hierarchical learning trajectory. Across training, model-brain alignment for both objectives shifted from lower-order sensory cortices towards language and association systems. Early-aligned representations were concentrated in sensory-motor regions, consistent with encoding of surface stimulus properties (Brincat et al., 2018) at the beginning of learning. Later-aligned representations became more prominent in language-related and higher-order associative regions, consistent with the emergence of a more abstract and integrated representational geometry that can support grammatical structure and generalization (Courellis et al., 2024; Johnston & Fusi, 2023). This interpretation fits prior evidence that language comprehension is organized along a cortical hierarchy, from acoustic and perceptual features to lexical, compositional and contextual representations (Caucheteux & King, 2022; De Heer et al., 2017), and that model-brain alignment is strongest when models capture hierarchical and contextual computations in higher-order language and association networks (Caucheteux et al., 2023; Mischler et al., 2024; Tang et al., 2023). Our results extend this work by showing that a similar progression of sensory-to-association representational alignment can be observed during learning itself, not only during mature language comprehension.

Individualized modeling highlights the role of feedback-related neural responses in explaining individual variations in learning outcomes. Early behavioral data alone provided only modest predictive power for later generalization, whereas models using early neural data performed significantly better, especially with feedback-related alignment (outcome prediction improved from $r = 0.27$ to $r = 0.43$). This clarifies the relative prediction-feedback dissociation by showing that the signal most strongly aligned with shared neural geometry is not necessarily the one that best predicts

individual learning outcomes. Prior work has shown that model-brain alignment varies across individuals, and the degree of alignment can correlate with humans' language comprehension performance (Caucheteux et al., 2022; Schrimpf et al., 2021). Here, we extend that logic to longitudinal learning outcomes. By combining early behavioral responses with participant-specific early neural targets compressed into the model's representational space, we were able to predict later generalization performance more accurately than early behavior alone. This improvement highlights the value of neural information for forecasting future learning outcomes, consistent with previous work showing that early distributed neural patterns contain information about individual language-learning profiles and later achievement (Feng, Ou, et al., 2021; Morgan-Short, 2020; Song et al., 2025).

This dissociation is psychologically plausible because prediction and feedback place different constraints on learning. Prediction-based signals may support the construction of structured internal representations that are useful across items, stages and learners, providing a common representational scaffold for extracting the grammar of a new language. Feedback-related signals, by contrast, may be more sensitive to learner-specific differences in how errors, correctness information and performance monitoring are used to update behavior. These differences may become especially consequential when learners must move beyond trained items and generalize abstract constraints to novel materials. Some learners may use feedback to infer the underlying structure of the language, whereas others may treat feedback as item-specific correction, leading to weaker transfer. From this perspective, feedback is not simply a weaker or secondary learning signal; rather, it carries information about individual learning efficiency.

More broadly, these findings reposition model-brain alignment as a mechanistic tool for studying language learning. Prior work has largely used alignment to evaluate whether artificial models resemble human neural responses during language processing. In the present study, alignment is used to adjudicate among candidate learning signals (Kriegeskorte, 2008; Kriegeskorte & Kievit, 2013). Because the transformer architecture and training materials were held constant, differences in model-brain alignment can be attributed more directly to the learning objectives imposed on the models. This makes it possible to ask not simply which model is more brain-like, but which computational pressure best explains shared neural geometry and learner-specific generalization. Thus, the study extends model-brain alignment from a method for comparing artificial and biological representations to a framework for testing how adults acquire new linguistic structure and why learners exposed to the same input diverge in later outcomes.

Several limitations should be considered when interpreting these findings. First, Brocanto2 offers strong experimental control over input, learners' prior training history, and grammatical structure, but it is still an artificial language with a limited lexicon and a simplified learning context (Morgan-Short et al., 2010, 2012). The extent to which the current findings generalize to naturalistic language learning remains open. Second,

our comparison is between matched learning objectives, not between exhaustive implementations of full theoretical frameworks. The findings therefore support complementary roles of prediction-based and feedback-based learning signals as operationalized here, rather than definitively resolving predictive-coding theory or reinforcement learning in general. Third, participants' neural data were collected during early learning, whereas the full behavioral learning experiment unfolded over seven days. Repeated neuroimaging across the full training period would provide a stronger test of how the balance between prediction and feedback signals changes over time. Finally, although humans and models were matched on materials and overall task structure, they were not matched on all aspects of exposure and learning dynamics, such as the number of repeated exposures required to reach maximum performance. Future work should test whether the same pattern holds with richer linguistic input, longer training windows and more naturalistic tasks.

In summary, this study reveals complementary contributions of prediction- and feedback-related signals. Representations optimized for prediction best accounted for the neural geometry shared across learners during early acquisition, whereas feedback-related neural signals more strongly predicted variability in later generalization. These findings support a multi-signal framework of adult language learning. More broadly, this work shows that model-brain alignment during learning can move beyond descriptive comparison, providing a principled approach for testing how candidate learning mechanisms shape the acquisition of new structural knowledge and why learners differ in their outcomes.

Methods

Participants

One hundred and six healthy adults from the community surrounding South China Normal University (mean age = 21.42 years; 73 females) participated in this study. All were native Mandarin speakers with formal training in English as a second language. None had formally studied a Romance language or been exposed to similar languages for more than three weeks. Four participants started the experiment, but later withdrew. All reported normal hearing and no history of neurological disorders. The study was approved by the Joint Chinese University of Hong Kong (CUHK) - New Territories East Cluster (NTEC) Clinical Research Ethics Committee (CREC) and the Research Ethics Committee at South China Normal University. Informed consent was obtained from each participant. Participants received monetary compensation upon completion.

Materials

Brocanto2 is a miniature artificial language designed to preserve key properties of natural language while allowing tight experimental control. It is fully productive, can be spoken and comprehended, and embeds lexical and grammatical structures in a meaningful board-game context (Fig. 2a), enabling learners to acquire form-meaning mappings in a constrained yet communicative setting. Prior neuroimaging studies using Brocanto and Brocanto2 have shown natural-language-like neural responses during processing, supporting their use as controlled models of adult language learning (Friederici et al., 2002; Morgan-Short et al., 2010, 2012; Opitz & Friederici, 2003).

The Brocanto2 lexicon comprised 13 lexical items, including four nouns (pleck, neep, blom, vode), two adjectives with gender-marked forms (troise/troiso, neime/neimo), one gender-marked article (li/lu), four verbs (klin, nim, yab, praz) and two adverbs (noyka, zayma). Nouns refer to game tokens and carry formal grammatical roles; verbs refer to actions; adjectives encode token shapes, and adverbs encode movement directions. Articles and adjectives were post-nominal and agreed in gender with the noun, sentences followed a fixed subject-object-verb (SOV) order, and adverbs, when present, immediately followed the verb. To minimize prosodic cues, all words were recorded in isolation and then presented sequentially. In the present study, the materials were organized into three construction types: noun phrases (NPs), simple subject-verb phrases (SVP), and SOV sentences.

Procedure

Participants completed seven consecutive days of Brocanto2 training. They also completed one auditory and one speech category-learning task for other research purposes. Neuroimaging data were acquired on Day 1, and behavioral training continued across the remaining sessions. Each daily session comprised a vocabulary-exposure phase followed by three grammar-learning tasks targeting NP, SVP, and SOV constructions. On Day 7, participants additionally completed feedback-free generalization tests on novel items. Training and test procedures were implemented in

E-Prime (Psychology Software Tools, Inc.) and were adapted from the Brocanto2 learning paradigm used in our earlier work (Feng, Ou, et al., 2021).

At the start of each session, participants completed a passive vocabulary-exposure phase in which each Brocanto2 lexical item was presented auditorily together with its corresponding visual referent. Grammar learning then proceeded as a grammaticality judgment task with trial-by-trial corrective feedback. No explicit grammatical rules were provided at any point. Instead, participants heard each phrase or sentence while viewing the corresponding game token or movement and judged its acceptability based on their immediate intuition. On-screen feedback then indicated whether the response was correct and served as the learning signal for subsequent trials (Fig. 2a).

Grammar learning trials were organized into six blocks per session, with two blocks for each construction type. Blocks were presented in a fixed order from simpler to more complex structures (i.e., from NP to SVP, then to SOV). Each block included 48 items, half grammatical and half ungrammatical, presented in random order. Ungrammatical items were generated by adding a single violation to an otherwise correct phrase or sentence. Consistent with Brocanto2 morphosyntax, violations targeted gender agreement in NPs and word-order rules in SVP and SOV constructions. During learning, the visual display always matched the intended meaning of the auditory item; thus, the task required grammaticality judgments rather than sentence-picture verification.

Each grammar-learning trial began with a 100-ms fixation cross, followed by a 100-ms blank interval. The auditory stimulus was then presented alongside the corresponding visual display. Stimulus duration varied by construction type: 2,400 ms for NPs, 6,300 ms for SVP items, and 7,600 ms for SOV sentences. After stimulus offset, a question mark prompted the participant to judge grammaticality. Corrective feedback (✓ or ×) was displayed for 1,000 ms after the response. To improve the separation of stimulus-related from feedback-related BOLD responses, the interval between response and feedback was jittered from 0 to 4,000 ms, and the inter-trial interval ranged from 2,000 to 6,000 ms.

On Day 7, participants completed a feedback-free grammaticality judgment generalization test assessing transfer of the learned grammar to new Brocanto2 items. In this test, participants judged 144 previously unseen phrases or sentences, including 72 grammatical and 72 ungrammatical items. As in training, each ungrammatical item contained a single violation. The visual displays matched the sentence meaning in all trials, so successful performance depended on identifying grammatical errors rather than semantic mismatches. Participants also completed a picture-sentence mapping test on Day 7 to assess whether spoken Brocanto2 sentences accurately described game tokens or movements. The trial structure matched that of the grammaticality judgment task. Although this task was used to evaluate broader generalization, its data were not included in the current analysis.

Image acquisition

Neuroimaging data were acquired during the Day-1 language training using a Siemens 3T MRI scanner at the Brain Imaging Center of South China Normal University. Functional and structural images were collected with a 20-channel head coil. Task-based functional images were acquired during the Brocanto2 vocabulary and grammar learning tasks using an interleaved whole-brain echo-planar imaging sequence. Each functional volume contained 56 slices, each 2 mm thick. The acquisition parameters were: repetition time = 2,000 ms, echo time = 30 ms, flip angle = 90°, field of view = 224 × 224 mm², and in-plane resolution = 2 × 2 mm².

High-resolution T1-weighted anatomical images were acquired in the sagittal plane using a magnetization-prepared rapid acquisition gradient-echo sequence, with the following parameters: repetition time = 1,900 ms, echo time = 2.53 ms, flip angle = 9°, and voxel size = 1 × 1 × 1 mm³. Resting-state fMRI and diffusion tensor imaging data were also collected during the same scanning session.

Brain image preprocessing

MRI data were preprocessed using fMRIPrep v23.2.1. T1-weighted images were bias-corrected, skull-stripped, segmented into cerebrospinal fluid, white matter, and gray matter, and normalized to MNI space. For each BOLD run, a reference image was coregistered to the T1-weighted image, and head motion was estimated with MCFLIRT. Functional images were resampled to native and MNI space. Nuisance regressors included framewise displacement, DVARS, mean cerebrospinal fluid, white matter, and whole-brain signals, as well as temporal and anatomical CompCor components explaining 50% of the variance. Motion and global signal regressors were expanded with temporal derivatives and quadratic terms, and volumes with framewise displacement greater than 1.0 mm were flagged as motion outliers. All spatial transformations were applied in a single interpolation step using `antsApplyTransforms` with Lanczos interpolation.

Language model training

We trained three customized GPT-style models (i.e., GPT-P, GPT-F and GPT-PF) using Python’s *transformers* library v4.42.4. All models shared the same backbone architecture, comprising one embedding layer and two decoder-only Transformer blocks, and differed only in their output heads and training objectives. GPT-style models provide a standard autoregressive architecture for next-token prediction, and the *transformers* library also supports sequence-classification heads for GPT-based models. We used byte-pair encoding for tokenization, together with special tokens such as `<s>` and `</s>`, yielding a vocabulary of 79 tokens.

GPT-P was trained with a next-token prediction objective using cross-entropy loss. GPT-F was trained with a binary classification head to judge whether each input sequence was grammatical or ungrammatical. GPT-F was also optimized with cross-entropy loss rather than a standard reinforcement-learning objective (e.g., value learning or policy optimization). We therefore refer to it as a feedback-based model because its supervision mirrors the trial-by-trial correctness feedback provided in the

human task. In this binary judgment task, explicit correctness feedback served as instructional information (Barto, A. G. & Dietterich, T. G., 2004) that directly specified the desired response rather than functioning only as a scalar reward signal. To include a control model that more closely aligns with the traditional computational definition of reinforcement learning, we also trained GPT-R using a policy-gradient algorithm (Williams, 1992; see Fig. S5).

Finally, the GPT-PF combined the next-token prediction and grammaticality classification objectives within a single model. The combined loss was defined as $L_{combined} = \alpha L_P + L_F$. To prevent the easier binary classification objective from dominating training, the prediction loss was weighted more heavily when generation accuracy lagged behind classification performance. Consistent with this rationale, we used $\alpha = \ln(\frac{79}{2})$ when the generation accuracy was lower than the classification accuracy, and $\alpha = 2$ otherwise. This weighting reflects the difference in baseline task difficulty between 79-way next-token prediction and binary grammaticality classification, and also compensates for the smaller amount of grammatical training data available for the prediction objective. Using the same training strategy, we trained a GPT-PR to combine the prediction and reward-based grammaticality classification objectives within a single model.

To assess model training performance, we asked GPT-P to generate outputs for all 1,092 items in the exhaustively constructed Brocanto2 corpus. We evaluated the model’s generalization ability as the percentage of generated sentences that were both novel (unseen by the model) and grammatical (i.e., “Gen accuracy”). GPT-F was evaluated using grammaticality-classification accuracy on a held-out 20% validation set, and GPT-PF/PR was evaluated using both metrics.

All three models were trained on datasets intended to approximate the overall scale of human exposure, while differing in the composition of the training input according to their learning objectives. The full training corpus contained grammatical and ungrammatical Brocanto2 sentences in a 1:1 ratio, matching the distribution that human participants encountered during learning. GPT-P was trained only on grammatical sentences, consistent with its generative objective, whereas GPT-F and GPT-PF were trained on 80% of the full corpus, including both grammatical and ungrammatical items. Each model was trained for 200 epochs with a learning rate of 5×10^{-4} , and the checkpoint with the best validation performance was used for subsequent analyses. Training was conducted on a single NVIDIA RTX A6000 GPU.

As an additional control, we trained a prediction model, GPT-P(L), on a corpus comprising the 144 grammatical Brocanto2 items and minimally corrected versions of the 144 ungrammatical items, thereby matching the number of training items used for GPT-F. All inputs to this control model were therefore grammatical, as in GPT-P, but the corpus size increased from 144 to 288 items. GPT-P(L) showed a model training trajectory broadly similar to that of the main GPT-P model and reached a peak generation accuracy of 0.94 (Supplementary Fig. S4).

Model performance and changes in internal representations

To test whether updates in model representations predicted changes in model behavior during training, we analyzed checkpoints prior to the best-performing checkpoint for each model. For each model, we repeated a resampling procedure 1,000 times. In each repetition, 12 checkpoints were randomly sampled. For each checkpoint, all 288 Brocanto2 items were passed through the model, and the final-token hidden-state vector was extracted from each layer, including the embedding layer and the two hidden transformer layers.

For each checkpoint pair, we quantified representational updating by subtracting the item-wise hidden-state vectors at the earlier checkpoint from those at the later checkpoint. This produced a representational-change vector for each item. We then computed an item-by-item representation-update RDM using Euclidean distances between these change vectors.

Model performance was quantified on the same 288 items and across the same checkpoint pairs. For GPT-P, performance updating was defined as the change in item-level sentence-generation probability, computed as the mean log probability of the sentences. For GPT-F, performance updating was defined as the change in grammaticality-judgment output (i.e., grammatical or ungrammatical). For GPT-PF, performance updating was computed separately for the generation branch and the grammaticality-judgment branch, and also for a combined measure obtained by averaging the z-scored changes from the two branches. For each performance measure, we constructed a performance-update RDM using Euclidean distance.

Finally, for each checkpoint pair and layer, we correlated the representational-update RDM with the corresponding performance-update RDM using Spearman correlation. Within each repetition, correlations were averaged across all checkpoint pairs to obtain one summary value per layer and behavioral measure. The resulting 1,000 resampled values were used to estimate the stability of the representation-performance coupling and to compare this coupling across layers and models.

Model-brain alignment with representational similarity analysis (RSA)

We used RSA to compare the geometry of the model and neural representations during language learning. RSA provides a common framework for comparing representational structures across computational models and brain activity, and Euclidean distance is widely used in searchlight-based multivoxel analyses when both spatial patterns and response magnitudes may carry information. For each Brocanto2 phrase or sentence, the full token sequence was passed through each trained model, and the hidden state at the final token was extracted from each model layer (the embedding layer plus two GPT hidden layers) as the sequence representation. Layer-specific model RDMs were then constructed across stimuli using cosine distance. To analyze training-related representational changes, we selected four checkpoints along each model's performance trajectory, yielding three consecutive training stages. For GPT-P, these checkpoints corresponded to generation accuracies of 0.33, 0.52, 0.71, and 0.91; for

GPT-F, they corresponded to classification accuracies of 0.51, 0.67, 0.83, and 1.00. At each stage, we calculated checkpoint-to-checkpoint difference vectors in hidden-state space and built representational-update RDMs using Euclidean distance, which measures the extent of representational change across training.

For the neural data, RDMs were computed from stimulus-specific t maps estimated with Nilearn (v0.10.3). Whole-brain RSA was implemented using a searchlight procedure in native space, with a 10-mm spherical region centered on each voxel. Within each searchlight, Euclidean distance quantified dissimilarity among local multivoxel activity patterns, and the resulting maps were transformed to standard space. We then performed two multiple-regression RSA analyses. In the cross-layer analysis, each neural RDM was regressed onto the two layer-specific RDMs from the same model. In the representational-update analysis, each neural RDM was regressed onto the three stage-specific update RDMs from a single layer. In both analyses, we included three control RDMs: an untrained GPT exposed to the same inputs, to account for representational structure attributable to architecture and stimulus exposure alone; a stimulus-length RDM, to account for variance related to sequence length and associated processing demands; and a block-identity RDM, to account for variance attributable to the experimental block structure. These controls were included to isolate model-brain alignment specific to the learned representational geometry rather than to generic architectural or design-related similarities. Group-level significance was assessed with threshold-free cluster enhancement (TFCE) and permutation testing (10,000 permutations; family-wise error-corrected $p < 0.05$) (Nichols & Holmes, 2002; Smith & Nichols, 2009).

To characterize alignment dynamics across brain networks, we additionally performed network-level RSA as part of the representational update analysis. The brain was parcellated into 12 functional networks using the Ji et al. (2019) atlas. Neural RDMs were computed within each network using Euclidean distance, and alignment with the three stage-specific update RDMs was assessed with partial Pearson correlations. This analysis estimated the unique contribution of each training stage while controlling for the other two stages.

Individualized neurocomputational modeling with neural, behavioral, and language data

Unlike the earlier GPT models, which were optimized for corpus-level performance, the individualized models were designed to additionally capture participant-specific behavioral and neural structures to predict later generalization outcomes and to examine whether prediction- or feedback-related neural signals explained individual differences in learning.

To incorporate neural signals into the models, we trained a self-supervised autoencoder to compress each participant's high-dimensional brain data into a lower-dimensional representation matched to the dimensionality of GPT's hidden states. This compressed neural representation was then used as an additional training target.

Although linear mapping approaches are commonly used to relate brain activity to computational models, they are limited in capturing nonlinear structure in large-scale neural data. By contrast, the autoencoder-based approach was intended to preserve the underlying nonlinear geometry in neural representations and, crucially, enabled joint optimization of multiple objectives within a single framework: predicting behavior, predicting the next token, and approximating neural activity (Han et al., 2019; Huang et al., 2018). ROIs were defined using brain masks derived from significant regions in the late stage of the representational-update analysis. Individualized models were then trained using prediction-related brain masks, feedback-related brain masks or their combination, allowing us to test which type of neural information best accounted for inter-learner variability (Fig. 5a).

For each participant, we trained a participant-specific GPT model with three joint objectives: predicting that participant’s grammaticality judgments during early learning (Days 1-2), fitting early neural responses from selected brain regions, and predicting the next token in Brocanto2 sequences. Because the neural data in standard space were much higher-dimensional than the model hidden state (271,633 voxels versus 768 units), we first compressed the neural data with the autoencoder (Han et al., 2019; Huang et al., 2018). The autoencoder comprised three fully connected layers, with a 768-dimensional bottleneck matched to the GPT hidden size. For each participant, it was trained on the other 101 participants in a leave-one-subject-out procedure and then applied to the held-out participant to generate low-dimensional neural targets. This approach ensures dimensionality transformation while preserving as much information as possible from the original neural data.

The individualized GPT was optimized with a weighted multitask objective, $L_{\text{combined}} = \alpha L_{\text{behavior}} + \beta L_{\text{neural}} + \gamma L_{\text{predict}}$, where L_{behavior} was the cross-entropy loss for participant-specific judgment prediction, L_{neural} was the mean-squared error between the model’s final-layer hidden states and the compressed neural data, and L_{predict} was the cross-entropy loss for next-token prediction. This weighted-sum formulation is standard in multitask learning when objectives differ in type and scale, but the exact coefficients are heuristic balancing hyperparameters rather than quantities with a unique theoretical optimum (Ruder, 2017). We set $\gamma = 1$ as the reference weight for the language-model objective. We set $\alpha = \ln(79/2)$ to upweight the behavioral term relative to next-token prediction, linking the weight to the difference in baseline cross-entropy between a 79-way token-prediction problem and a binary judgment problem. We set $\beta = 4/768$ as a small scaling factor to keep the neural regression term numerically comparable to the two cross-entropy losses. Behavioral supervision used each participant’s observed responses on Days 1 and 2; to reduce day-specific overfitting, training alternated between Day 1 and Day 2 response labels every 30 epochs.

For each participant, Day-1 and Day-2 data were split into 70% for training and 30% for held-out validation. Models were trained for 100 epochs, and the checkpoint with the highest held-out behavioral accuracy was retained. The retained individual

models were then used to predict grammaticality judgments in the Day-7 generalization task, testing whether early behavioral and neural signals forecast later responses to novel items for each individual learner. A significant correlation between model-predicted and observed human generalization performance was taken as evidence of successful individualized modeling and suggested that information from the corresponding brain regions contributed to predicting individual differences in learning outcomes.

Data availability

De-identified behavioral data, model-derived representations and group-level statistical maps will be deposited on OSF before publication.

Code availability

The code for replicating the main analyses of this paper is available at: https://github.com/thedarkkinght/GPTs_learn_Brocanto2

Author contributions: Shu.Y. and G.F. designed research; Shu.Y., X. J., and S.W. performed research; Shu.Y. and Shao.Y. analyzed data; Shu.Y. and G.F. wrote the first draft of the paper; Shu.Y., Shao.Y., and G.F. edited the paper; Shu.Y. and G.F. wrote the paper.

Supplementary Materials

Supplementary Figures

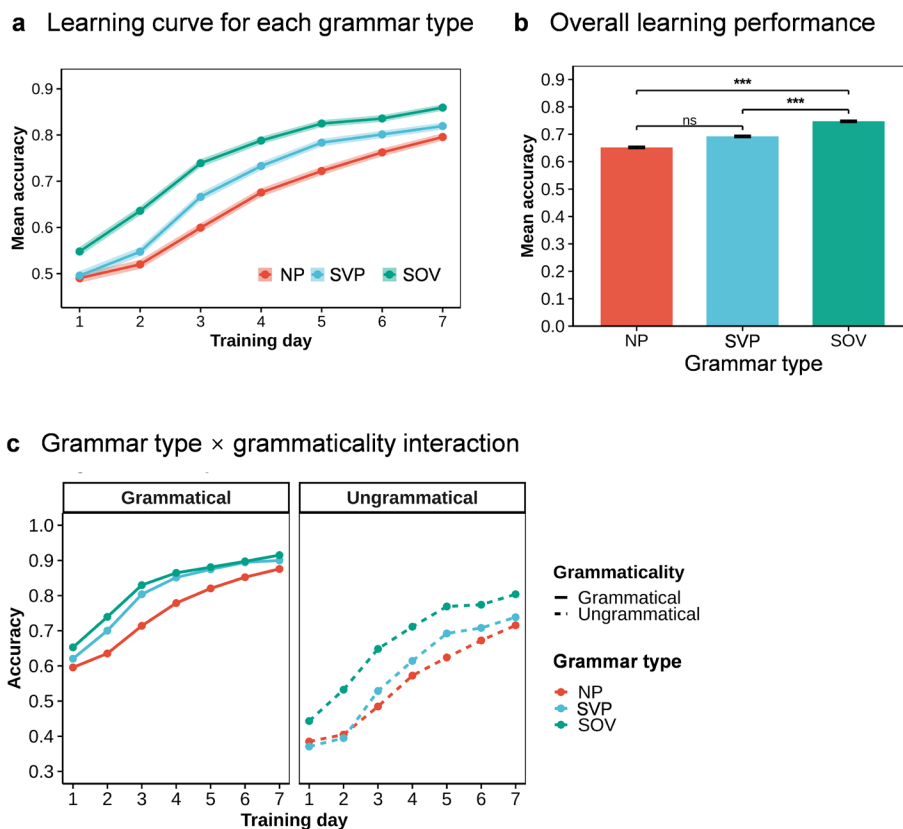


Fig. S1. Behavioral learning across training days. Trial-level accuracy was analyzed with a mixed-effects logistic regression including random intercepts for participants and items. **a**, Accuracy improved across the 7-day training period for all construction types, with the highest performance for SOV, followed by SVP and NP. **b**, Main effect of construction type. Bonferroni-corrected pairwise comparisons showed that SOV accuracy was higher than SVP ($\beta = 0.52$, $p < 0.001$, OR = 1.69) and NP ($\beta = 0.55$, $p < 0.001$, OR = 1.74), whereas SVP and NP did not differ. **c**, Construction type × grammaticality interaction. Accuracy was higher for grammatical than ungrammatical items overall ($\beta = 1.09$, $p < 0.001$, OR = 2.96), and this grammaticality effect differed across construction types ($\chi^2(2) = 6.18$, $p = 0.045$). Accuracy also increased reliably across days ($\beta = 0.29$, $p < 0.001$), with faster improvement for SVP and SOV than NP (SVP × Day: $\beta = 0.042$, $p < 0.001$; SOV × Day: $\beta = 0.031$, $p < 0.001$).

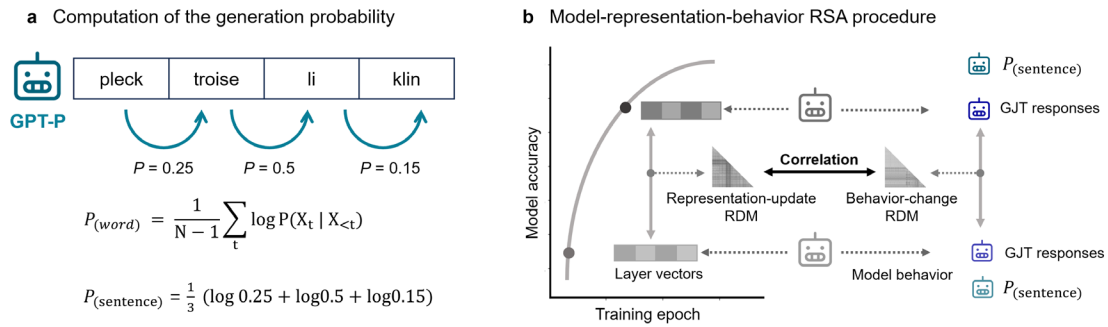
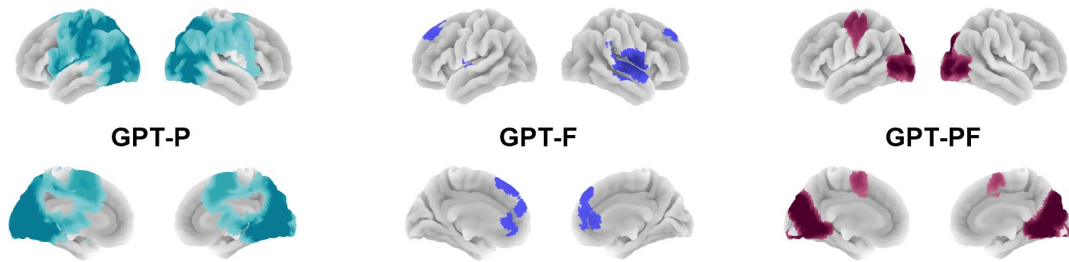
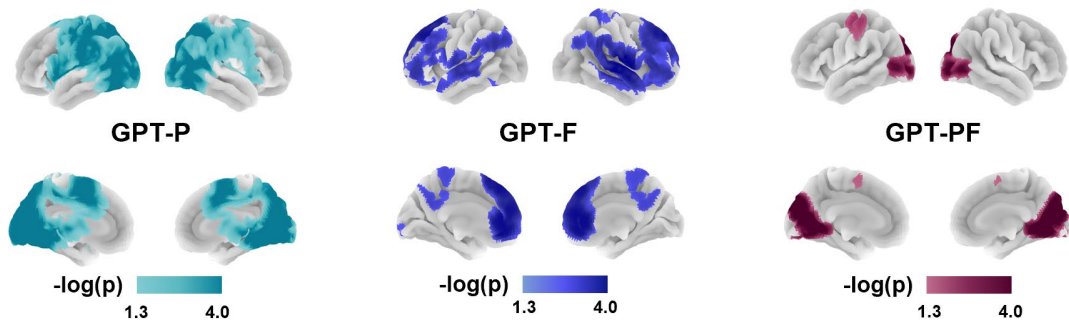


Fig. S2. Similarity analysis procedure to examine the relationship between model representational updates and behavioral changes. **a**, Item-level behavioral scores for GPT-P were computed from the mean sentence log probability, obtained by averaging token-wise conditional log probabilities across each Brocanto2 sequence. This score indexed the model’s generative behaviors for each item. **b**, Model-representation-behavior RSA procedure. For each pair of training checkpoints, representational updating was computed as the item-wise difference between layer vectors for each model layer. Behavioral updating was computed using the same checkpoint pair from item-level model outputs: mean sentence log probability for GPT-P, grammaticality judgment responses for GPT-F, and the corresponding generation, classification, and combined scores for GPT-PF. Representational-update and behavior-update RDMs were constructed across the 288 Brocanto2 items using Euclidean distance, and their correspondence was assessed using Spearman's rank correlation.

a Model-brain alignment (Layer 1)



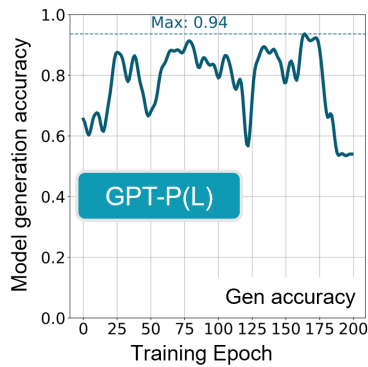
b Model-brain alignment (Layer 2)



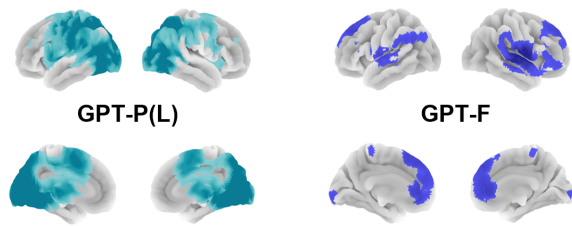
(FWE-corrected $p < 0.05$)

Fig. S3. Layer-wise model-brain representational alignment. **a,b**, Whole-brain searchlight RSA results for the first (a) and second (b) hidden layers of GPT-P, GPT-F and GPT-PF. Model RDMs were fitted to fMRI-derived neural RDMs while controlling for an untrained GPT baseline, stimulus length and block identity. GPT-P showed broad alignment across both layers. GPT-F showed weaker, more spatially restricted alignment in layer 1 but stronger alignment in layer 2. GPT-PF showed significant alignment in both layers, with a more focal spatial pattern in sensorimotor regions. Brain maps were thresholded using TFCE with 10,000 permutations and family-wise-error correction at $p < 0.05$. Color bars indicate $-\log(p)$.

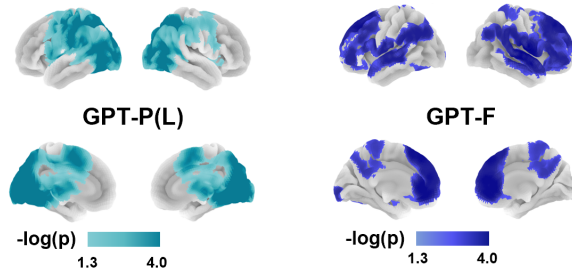
a GPT-P(L) training trajectory



b Model-brain alignment (Layer 1)



c Model-brain alignment (Layer 2)



(FWE-corrected $p < 0.05$)

Fig. S4. Control prediction model trained on an expanded grammatical corpus. **a**, training trajectory of GPT-P(L), a prediction model trained on the original 144 grammatical Brocanto2 items plus 144 minimally-corrected grammatical versions of ungrammatical items. GPT-P(L) showed a model training trajectory similar to the main GPT-P model and reached a peak generation accuracy of 0.94. **b, c**, Whole-brain model-brain alignment results for layer 1 (**b**) and layer 2 (**c**). GPT-P(L) was compared with the same GPT-F models used in the main analysis. Consistent with the main prediction-model findings, GPT-P(L) showed robust and spatially extensive alignment with human neural representations across layers. Brain maps were thresholded using TFCE with 10,000 permutations and family-wise-error correction at $p < 0.05$. Color bars indicate $-\log(p)$.

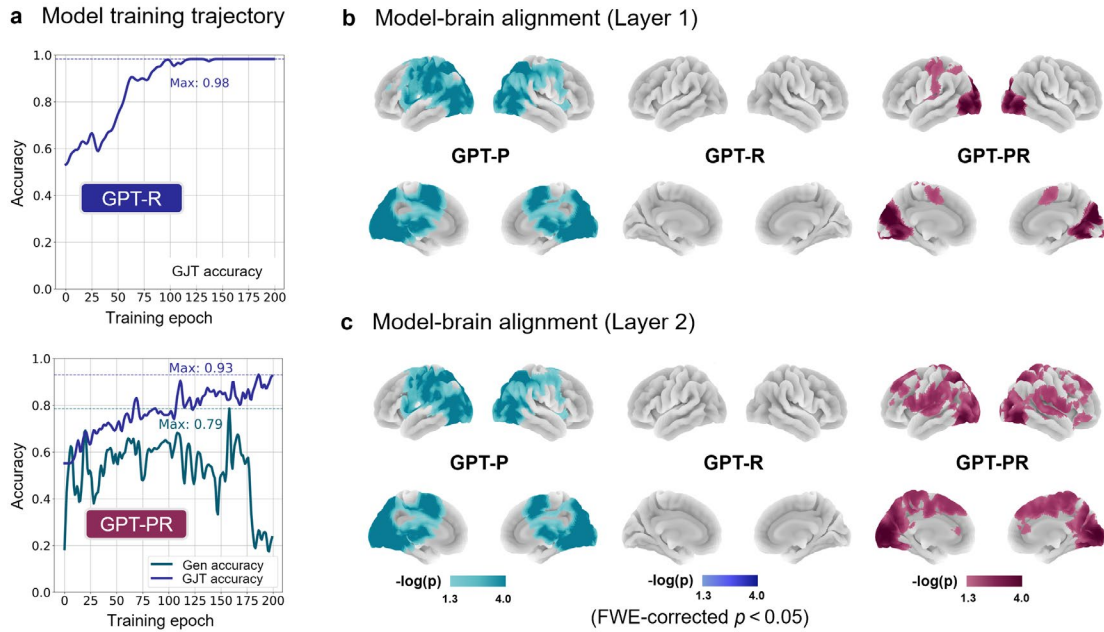


Fig. S5. Policy-gradient control models and model-brain alignment. **a**, Validation performance across training epochs for the policy-gradient grammaticality model, GPT-R, and the combined prediction-plus-policy-gradient model, GPT-PR. GPT-R was evaluated by grammaticality-classification accuracy and reached a maximum accuracy of 0.98. GPT-PR was evaluated on both grammaticality classification accuracy and generation accuracy, achieving a maximum classification accuracy of 0.93 and a maximum generation accuracy of 0.79. **b**, **c**, Whole-brain RSA results for the first (**b**) and second (**c**) hidden layers. GPT-P showed significant model-brain alignment in both layers, whereas GPT-R showed no suprathreshold alignment despite high task accuracy. GPT-PR showed significant alignment, particularly in the second layer. Brain maps were thresholded using TFCE with 10,000 permutations and family-wise-error correction at $p < 0.05$. Color bars indicate $-\log(p)$; grey indicates no suprathreshold voxels. These results indicate that policy-gradient task learning alone was insufficient to reproduce human neural representational geometry, whereas alignment emerged when policy-gradient learning was combined with a prediction objective.

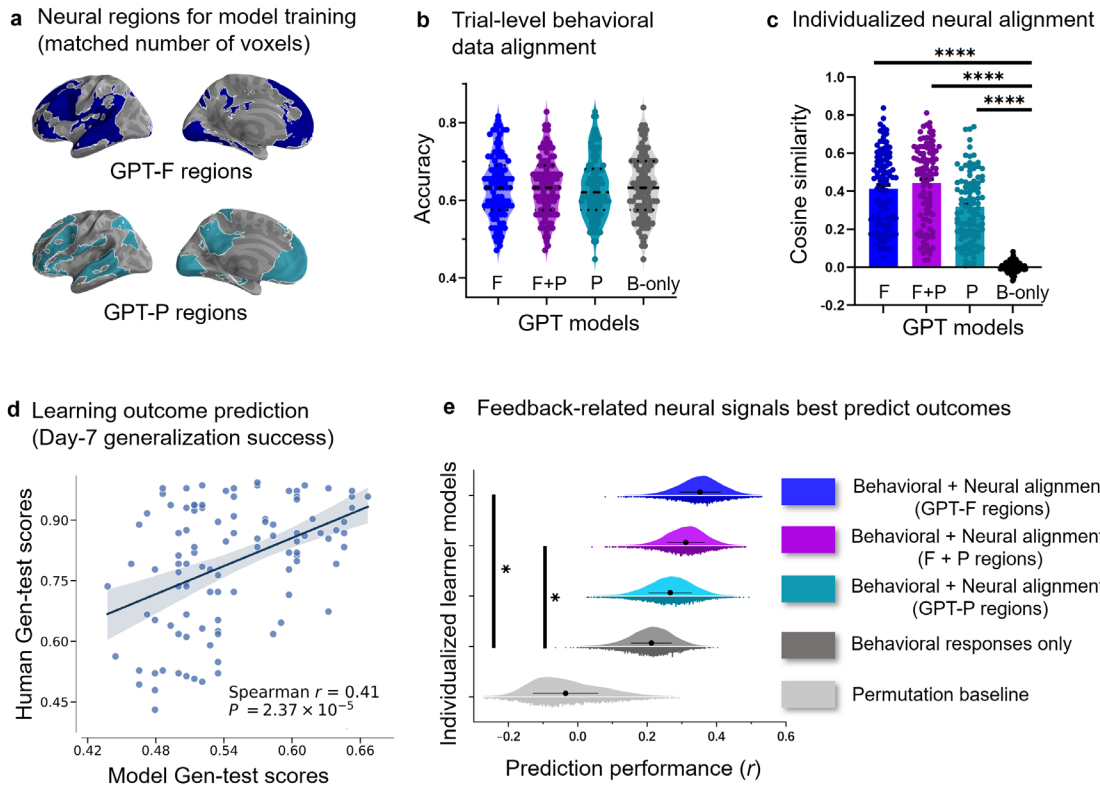


Fig. S6. Voxel-matched control analysis for individualized model prediction. **a**, Prediction- and feedback-aligned neural masks (derived from the update RSA results) used for individualized model training. The feedback-aligned mask was threshold-adjusted to match the voxel count of the prediction-aligned mask. **b**, Trial-level consistency between individualized model predictions and participants' grammaticality judgments during early training (i.e., days 1 and 2). **c**, Neural alignment of individualized models, measured as cosine similarity between model hidden representations and participant-specific compressed neural targets. Bars show group means; dots indicate participants. **d**, Association between model-predicted and observed Day 7 generalization performance. Each dot represents a participant; the line shows the fitted association. Spearman's r and p values are reported. **e**, Bootstrap distributions of prediction performance across 10,000 resamples. Asterisks indicate models whose median correlation exceeded the 95th percentile of the behavioral-only baseline.

References

- Arbel, Y., Hong, L., Baker, T. E., & Holroyd, C. B. (2017). It's all about timing: An electrophysiological examination of feedback-based learning with immediate and delayed feedback. *Neuropsychologia*, *99*, 179–186. <https://doi.org/10.1016/j.neuropsychologia.2017.03.003>
- Arbel, Y., Murphy, A., & Donchin, E. (2014). On the utility of positive and negative feedback in a paired-associate learning task. *Journal of Cognitive Neuroscience*, *26*(7), 1445–1453. https://doi.org/10.1162/jocn_a_00617
- Ashby, F. G., Alfonso-Reese, L. A., Turken, A. U., & Waldron, E. M. (1998). A neuropsychological theory of multiple systems in category learning. *Psychological Review*, *105*(3), 442–481. <https://doi.org/10.1037/0033-295x.105.3.442>
- Barto, A. G. & Dietterich, T. G. (2004). Reinforcement learning and its relationship to supervised learning. *Handbook of Learning and Approximate Dynamic Programming*. <https://doi.org/10.1109/9780470544785.ch2>
- Bovolenta, G., & Marsden, E. (2022). Prediction and error-based learning in L2 processing and acquisition: A conceptual review. *Studies in Second Language Acquisition*, *44*(5), 1384–1409. <https://doi.org/10.1017/S0272263121000723>
- Brincat, S. L., Siegel, M., Von Nicolai, C., & Miller, E. K. (2018). Gradual progression from sensory to task-related processing in cerebral cortex. *Proceedings of the National Academy of Sciences*, *115*(30), 1–10. <https://doi.org/10.1073/pnas.1717075115>
- Caucheteux, C., Gramfort, A., & King, J.-R. (2022). Deep language algorithms predict semantic comprehension from brain activity. *Scientific Reports*, *12*(1), 16327. <https://doi.org/10.1038/s41598-022-20460-9>
- Caucheteux, C., Gramfort, A., & King, J.-R. (2023). Evidence of a predictive coding hierarchy in the human brain listening to speech. *Nature Human Behaviour*, *7*(3), 430–441. <https://doi.org/10.1038/s41562-022-01516-2>
- Caucheteux, C., & King, J.-R. (2022). Brains and algorithms partially converge in natural language processing. *Communications Biology*, *5*(1), 134. <https://doi.org/10.1038/s42003-022-03036-1>
- Chang, F., Dell, G. S., & Bock, K. (2006). Becoming syntactic. *Psychological Review*, *113*(2), 234–272. <https://doi.org/10.1037/0033-295X.113.2.234>
- Chang, F., Kidd, E., & Rowland, C. F. (2013). Prediction in processing is a by-product of language learning. *Behavioral and Brain Sciences*, *36*(4), 350–351. Cambridge Core. <https://doi.org/10.1017/S0140525X12002518>
- Courellis, H. S., Minxha, J., Cardenas, A. R., Kimmel, D. L., Reed, C. M., Valiante, T. A., Salzman, C. D., Mamelak, A. N., Fusi, S., & Rutishauser, U. (2024). Abstract representations emerge in human hippocampal neurons during inference. *Nature*, *632*(8026), 841–849. <https://doi.org/10.1038/s41586-024-07799-x>
- De Heer, W. A., Huth, A. G., Griffiths, T. L., Gallant, J. L., & Theunissen, F. E. (2017). The hierarchical cortical organization of human speech processing. *The Journal of Neuroscience*, *37*(27), 6539–6557. <https://doi.org/10.1523/JNEUROSCI.3267-16.2017>

- Elman, J. L. (1990). Finding Structure in Time. *Cognitive Science*, *14*(2), 179–211. https://doi.org/10.1207/s15516709cog1402_1
- Feng, G., Gan, Z., Yi, H. G., Ell, S. W., Roark, C. L., Wang, S., Wong, P. C. M., & Chandrasekaran, B. (2021). Neural dynamics underlying the acquisition of distinct auditory category structures. *NeuroImage*, *244*, 118565. <https://doi.org/10.1016/j.neuroimage.2021.118565>
- Feng, G., Ou, J., Gan, Z., Jia, X., Meng, D., Wang, S., & Wong, P. C. M. (2021). Neural fingerprints underlying individual language learning profiles. *The Journal of Neuroscience*, *41*(35), 7372–7387. <https://doi.org/10.1523/JNEUROSCI.0415-21.2021>
- Friederici, A. D., Steinhauer, K., & Pfeifer, E. (2002). Brain signatures of artificial language processing: Evidence challenging the critical period hypothesis. *Proceedings of the National Academy of Sciences*, *99*(1), 529–534. <https://doi.org/10.1073/pnas.012611199>
- Friston, K. (2005). A theory of cortical responses. *Philosophical Transactions of the Royal Society B: Biological Sciences*, *360*(1456), 815–836. <https://doi.org/10.1098/rstb.2005.1622>
- Goldstein, A., Zada, Z., Buchnik, E., Schain, M., Price, A., Aubrey, B., Nastase, S. A., Feder, A., Emanuel, D., Cohen, A., Jansen, A., Gazula, H., Choe, G., Rao, A., Kim, C., Casto, C., Fanda, L., Doyle, W., Friedman, D., ... Hasson, U. (2022). Shared computational principles for language processing in humans and deep language models. *Nature Neuroscience*, *25*(3), 369–380. <https://doi.org/10.1038/s41593-022-01026-4>
- Groen, I. I., Greene, M. R., Baldassano, C., Fei-Fei, L., Beck, D. M., & Baker, C. I. (2018). Distinct contributions of functional and deep neural network features to representational similarity of scenes in human brain and behavior. *eLife*, *7*, e32962. <https://doi.org/10.7554/eLife.32962>
- Hagoort, P. (2019). The neurobiology of language beyond single-word processing. *Science*, *366*(6461), 55–58. <https://doi.org/10.1126/science.aax0289>
- Hamrick, P., Lum, J. A. G., & Ullman, M. T. (2018). Child first language and adult second language are both tied to general-purpose learning systems. *Proceedings of the National Academy of Sciences*, *115*(7), 1487–1492. <https://doi.org/10.1073/pnas.1713975115>
- Han, K., Wen, H., Shi, J., Lu, K.-H., Zhang, Y., Fu, D., & Liu, Z. (2019). Variational autoencoder: An unsupervised model for encoding and decoding fMRI activity in visual cortex. *NeuroImage*, *198*, 125–136. <https://doi.org/10.1016/j.neuroimage.2019.05.039>
- Heilbron, M., Armeni, K., Schoffelen, J.-M., Hagoort, P., & De Lange, F. P. (2022). A hierarchy of linguistic predictions during natural language comprehension. *Proceedings of the National Academy of Sciences*, *119*(32), e2201968119. <https://doi.org/10.1073/pnas.2201968119>
- Huang, H., Hu, X., Zhao, Y., Makkie, M., Dong, Q., Zhao, S., Guo, L., & Liu, T. (2018). Modeling Task fMRI Data Via Deep Convolutional Autoencoder. *IEEE Transactions on Medical Imaging*, *37*(7), 1551–1561.

- <https://doi.org/10.1109/TMI.2017.2715285>
- Huetting, F., & Mani, N. (2016). Is prediction necessary to understand language? Probably not. *Language, Cognition and Neuroscience*, 31(1), 19–31. <https://doi.org/10.1080/23273798.2015.1072223>
- Ito, A., Pickering, M. J., & Corley, M. (2018). Investigating the time-course of phonological prediction in native and non-native speakers of English: A visual world eye-tracking study. *Journal of Memory and Language*, 98, 1–11. <https://doi.org/10.1016/j.jml.2017.09.002>
- Ji, J. L., Spronk, M., Kulkarni, K., Repovš, G., Anticevic, A., & Cole, M. W. (2019). Mapping the human brain's cortical-subcortical functional network organization. *NeuroImage*, 185, 35–57. <https://doi.org/10.1016/j.neuroimage.2018.10.006>
- Johnston, W. J., & Fusi, S. (2023). Abstract representations emerge naturally in neural networks trained to perform multiple tasks. *Nature Communications*, 14(1), 1–18. <https://doi.org/10.1038/s41467-023-36583-0>
- Kidd, E., Donnelly, S., & Christiansen, M. H. (2018). Individual Differences in Language Acquisition and Processing. *Trends in Cognitive Sciences*, 22(2), 154–169. <https://doi.org/10.1016/j.tics.2017.11.006>
- Kriegeskorte, N. (2008). Representational similarity analysis – connecting the branches of systems neuroscience. *Frontiers in Systems Neuroscience*. <https://doi.org/10.3389/neuro.06.004.2008>
- Kriegeskorte, N., & Kievit, R. A. (2013). Representational geometry: Integrating cognition, computation, and the brain. *Trends in Cognitive Sciences*, 17(8), 401–412. <https://doi.org/10.1016/j.tics.2013.06.007>
- Krishnan, S., Watkins, K. E., & Bishop, D. V. M. (2016). Neurobiological Basis of Language Learning Difficulties. *Trends in Cognitive Sciences*, 20(9), 701–714. <https://doi.org/10.1016/j.tics.2016.06.012>
- Menon, V. (2023). 20 years of the default mode network: A review and synthesis. *Neuron*, 111(16), 2469–2487. <https://doi.org/10.1016/j.neuron.2023.04.023>
- Minda, J. P., Roark, C. L., Kalra, P., & Cruz, A. (2024). Single and multiple systems in categorization and category learning. *Nature Reviews Psychology*, 3(8), 536–551. <https://doi.org/10.1038/s44159-024-00336-7>
- Mischler, G., Li, Y. A., Bickel, S., Mehta, A. D., & Mesgarani, N. (2024). Contextual feature extraction hierarchies converge in large language models and the brain. *Nature Machine Intelligence*, 6(12), 1467–1477. <https://doi.org/10.1038/s42256-024-00925-4>
- Morgan-Short, K. (2020). Insights into the neural mechanisms of becoming bilingual: A brief synthesis of second language research with artificial linguistic systems. *Bilingualism: Language and Cognition*, 23(1), 87–91. <https://doi.org/10.1017/S1366728919000701>
- Morgan-Short, K., Sanz, C., Steinhauer, K., & Ullman, M. T. (2010). Second Language Acquisition of Gender Agreement in Explicit and Implicit Training Conditions: An Event-Related Potential Study. *Language Learning*, 60(1), 154–193. <https://doi.org/10.1111/j.1467-9922.2009.00554.x>
- Morgan-Short, K., Steinhauer, K., Sanz, C., & Ullman, M. T. (2012). Explicit and

- Implicit Second Language Training Differentially Affect the Achievement of Native-like Brain Activation Patterns. *Journal of Cognitive Neuroscience*, 24(4), 933–947. https://doi.org/10.1162/jocn_a_00119
- Naselaris, T., Kay, K. N., Nishimoto, S., & Gallant, J. L. (2011). Encoding and decoding in fMRI. *NeuroImage*, 56(2), 400–410. <https://doi.org/10.1016/j.neuroimage.2010.07.073>
- Nichols, T. E., & Holmes, A. P. (2002). Nonparametric permutation tests for functional neuroimaging: A primer with examples. *Human Brain Mapping*, 15(1), 1–25. <https://doi.org/10.1002/hbm.1058>
- Opitz, B., & Friederici, A. D. (2003). Interactions of the hippocampal system and the prefrontal cortex in learning language-like rules. *NeuroImage*, 19(4), 1730–1737. [https://doi.org/10.1016/S1053-8119\(03\)00170-8](https://doi.org/10.1016/S1053-8119(03)00170-8)
- Pelucchi, B., Hay, J. F., & Saffran, J. R. (2009). Learning in reverse: Eight-month-old infants track backward transitional probabilities. *Cognition*, 113(2), 244–247. <https://doi.org/10.1016/j.cognition.2009.07.011>
- Rabagliati, H., Gambi, C., & Pickering, M. J. (2015). Learning to predict or predicting to learn? *Language, Cognition and Neuroscience*, 31(1), 94–105. <https://doi.org/10.1080/23273798.2015.1077979>
- Riesenhuber, M., & Poggio, T. (1999). Hierarchical models of object recognition in cortex. *Nature Neuroscience*, 2(11), 1019–1025. <https://doi.org/10.1038/14819>
- Ruder, S. (2017). *An Overview of Multi-Task Learning in Deep Neural Networks* (arXiv:1706.05098). arXiv. <https://doi.org/10.48550/arXiv.1706.05098>
- Saffran, J. R. (2002). Constraints on statistical language learning. *Journal of Memory and Language*, 47(1), 172–196. <https://doi.org/10.1006/jmla.2001.2839>
- Saffran, J. R., Aslin, R. N., & Newport, E. L. (1996). Statistical Learning by 8-Month-Old Infants. *Science*, 274(5294), 1926–1928. <https://doi.org/10.1126/science.274.5294.1926>
- Schrimpf, M., Blank, I. A., Tuckute, G., Kauf, C., Hosseini, E. A., Kanwisher, N., Tenenbaum, J. B., & Fedorenko, E. (2021). The neural architecture of language: Integrative modeling converges on predictive processing. *Proceedings of the National Academy of Sciences*, 118(45), e2105646118. <https://doi.org/10.1073/pnas.2105646118>
- Schultz, W., Dayan, P., & Montague, P. R. (1997). A neural substrate of prediction and reward. *Science*, 275(5306), 1593–1599. <https://doi.org/10.1126/science.275.5306.1593>
- Smith, S., & Nichols, T. (2009). Threshold-free cluster enhancement: Addressing problems of smoothing, threshold dependence and localisation in cluster inference. *NeuroImage*, 44(1), 83–98. <https://doi.org/10.1016/j.neuroimage.2008.03.061>
- Song, P., Yang, S., Geng, X., Gan, Z., Wang, S., & Feng, G. (2025). *Multi-network Topology Underlying Individual Language Learning Success* (arXiv:2511.14453). arXiv. <https://doi.org/10.48550/arXiv.2511.14453>
- Stolier, R. M., & Freeman, J. B. (2016). Neural pattern similarity reveals the inherent intersection of social categories. *Nature Neuroscience*, 19(6), 795–797. <https://doi.org/10.1038/nn.4296>

- Sutton, R. S., & Barto, A. G. (2018). *Reinforcement learning: An introduction*. The MIT Press.
- Tang, J., LeBel, A., Jain, S., & Huth, A. G. (2023). Semantic reconstruction of continuous language from non-invasive brain recordings. *Nature Neuroscience*, 26(5), 858–866. <https://doi.org/10.1038/s41593-023-01304-9>
- Ullman, M. T. (2004). Contributions of memory circuits to language: The declarative/procedural model. *Cognition*, 92(1–2), 231–270. <https://doi.org/10.1016/j.cognition.2003.10.008>
- Williams, R. J. (1992). Simple statistical gradient-following algorithms for connectionist reinforcement learning. *Machine Learning*, 8(3), 229–256. <https://doi.org/10.1007/BF00992696>